Research & Design of Nuclear Engineering, **1**, 2025009 (2025)

https://doi.org/10.1051/rdne/2025009

Available online at:
https://rdne.edpsciences.org/

RESEARCH ARTICLE OPEN ACCESS

Corrosion behavior of 000Cr25Ni20 and 304L stainless steels in boiling nitric acid solutions containing Ce^{4+} ions

Qiqian Chen[1,2], Aili Ma[1,*], Lianmin Zhang[1], and Yugui Zheng[1,*]

[1] Key Laboratory of Nuclear Materials and Safety Assessment, Institute of Metal Research, Chinese Academy of Sciences, 62 Wencui Road, Shenyang, 110016, PR China
[2] School of Materials Science and Engineering, University of Science and Technology of China, 72 Wenhua Road, Shenyang 110016, PR China

Received: 10 June 2025 / Accepted: 24 October 2025

Abstract. This study investigated the corrosion behavior of 000Cr25Ni20 (C25) and 304L stainless steels (SS) in boiling nitric acid solution containing Ce^{4+} ions. Open circuit potential, electrochemical impedance spectroscopy, potentiodynamic polarization, weight loss measurement, scanning electron microscopy, and energy dispersive spectroscopy were employed to elucidate the effects of Ce^{4+} ions and nitric acid concentration on the corrosion behavior of C25 and 304L SS. The results demonstrated that Ce^{4+} ions significantly accelerated the cathodic reaction, thereby markedly increasing the corrosion rates of both C25 and 304L SS. Both the cathodic reaction rate and the overall corrosion rate increased monotonically with increasing Ce^{4+} concentration. However, in the presence of Ce^{4+} ions, the effect of nitric acid concentration (3, 6, and 10 mol/L) on E_{corr}, I_{corr}, and R_p for both SS was negligible, indicating that the influence of nitric acid concentration was less significant compared to that of Ce^{4+} ions. The highest corrosion rates were observed during the initial 48-hour exposure cycle, followed by a decrease and stabilization in the subsequent four cycles. C25 exhibited superior corrosion resistance compared to 304L SS, suggesting its potential application in fabricating reprocessing equipment requiring higher corrosion resistance than 304L SS. These findings provide critical insights into operational monitoring and material selection for nuclear fuel reprocessing equipment.

Keywords: Stainless steel / Cerium ion / Nitric acid corrosion / Electrochemical behavior / Spent nuclear fuel reprocessing.

1 Introduction

Against the backdrop of global energy structure transformation, spent nuclear fuel reprocessing (SNFR) technology plays a crucial role in achieving a closed nuclear fuel cycle, enhancing resource utilization efficiency, and optimizing radioactive waste management. The Plutonium and Uranium Recovery by Extraction (PUREX) method, widely adopted as the core process for SNFR in countries such as France and Japan, involves dissolving spent nuclear fuel in concentrated nitric acid under high-temperature conditions. This process enables the separation of fission products and facilitates the efficient recovery of unused nuclear fuel, thereby significantly improving the efficiency of the nuclear fuel cycle and mitigating the challenges associated with waste disposal [1].

Traditional austenitic stainless steels (SS) are widely employed as structural materials in reprocessing plants due to their excellent corrosion resistance, favorable mechanical properties, and cost-effectiveness. However, stainless steels are susceptible to intergranular corrosion (IGC) in the high-temperature concentrated HNO_3 environment of reprocessing plants [2, 3]. Research has shown that the key factor driving IGC in SS within reprocessing solutions is the presence of significant quantities of oxidizing cations, such as Ru^{7+}, Cr^{6+}, and Ce^{4+} ions [4]. These oxidizing cations elevate the corrosion potential of stainless steel into the transpassive region through redox reactions, thereby significantly increasing the risk of IGC [5]. The reprocessing medium contains substantial amounts of cerium (Ce) derived from fission products [4, 6]. Moreover, Ce^{4+} ions are frequently used in laboratory-simulated reprocessing media as a substitute for radioactive Am^{3+} ions due to their comparable standard redox potentials: AmO_2^{2+}/AmO^{2+} (E^{Θ}=1.639 V)→Ce^{4+}/Ce^{3+}(E^{Θ} = 1.610 V), indicating that the role of Ce^{4+} ions in the reprocessing medium

* e-mail: alma@imr.ac.cn (Aili Ma); ygzheng@imr.ac.cn (Yugui Zheng)

cannot be overlooked. Nevertheless, the current corrosion research on stainless steel in a reprocessing environment containing Ce^{4+} ions remains controversial. On the one hand, the methods for introducing Ce^{4+} ions vary significantly across studies, with some studies adding Ce^{4+} ions independently [7], while most studies employ a mixed system comprising Ce^{4+} ions and other oxidizing species [6, 8]. Different experimental conditions lead to a lack of comparability among research findings. On the other hand, the role of Ce^{4+} ions in influencing the corrosion resistance of stainless steel remains inconclusive. For instance, Liu et al. [7] investigated the corrosion behavior of SiN SS in a 6 mol/L nitric acid solution containing Ce^{4+} ions and reported that the reduction products of Ce^{4+} ions could participate in the formation of passive film, thus inhibiting the corrosion of stainless steel. In contrast, Bhise et al. [6] studied the corrosion behavior of 304L SS in 6 mol/L HNO_3 containing V^{5+} and Ce^{4+} ions, revealing that the interaction between these oxidizing ions decreases the corrosion resistance. Additionally, Yamamoto et al. [8] demonstrated that the introduction of Ce^{4+}, Cr^{6+}, and Ru^{3+} ions accelerated the corrosion of 304L SS in a 9 mol/L HNO_3 solution. Therefore, further systematic research is essential to clarify the role of Ce^{4+} ions in the corrosion resistance of stainless steel under SNFR environments.

The HNO_3 concentrations exhibit significant dynamic fluctuations during the actual reprocessing operations [9, 10]. For example, medium-release evaporators and high-release waste evaporators are typically operated in a boiling 3 mol/L HNO_3 environment; continuous dissolvers function within a boiling 6 mol/L HNO_3 environment; and high-deuterated acid recovery evaporators operate under a boiling 10 mol/L HNO_3 condition. Gopinath et al. [11] demonstrated that the influence of oxidizing ions on the corrosion behavior in HNO_3 solutions varies with HNO_3 concentration. Specifically, increasing the HNO_3 concentration from 2 to 8 mol/L markedly decreased the corrosion resistance of 304L SS in solutions free of oxidizing ions or containing only Nd^{3+}, Mo^{6+}, and Cs^{+} ions. Conversely, enhanced corrosion resistance was observed in solutions containing Nd^{3+}, Mo^{6+}, Cs^{+}, and Fe^{3+} ions, indicating a synergistic effect between HNO_3 concentration and oxidizing ions that collectively influence the corrosion process. However, research into the mechanism of synergistic interaction between HNO_3 concentration and Ce^{4+} ions during the corrosion process remains scarce.

Furthermore, beyond the fluctuations in HNO_3 concentration, the chemical milieu of reprocessing plants can involve the presence of other acidic species during specific operational stages. For instance, hydrofluoric acid (HF) may be introduced to aid the dissolution of certain nuclear fuels, while oxalic acid might be used for precipitation or redox control [4, 12]. The introduction of these additional acids can profoundly impact corrosion behavior. HF, in particular, is highly aggressive as fluoride ions can effectively disrupt the protective passive films on stainless steels by forming soluble metal-fluoride complexes, potentially leading to severe general and localized corrosion [13]. While the synergistic effects of such acids with oxidizing ions like Ce^{4+} present a critical area for future investigation, the current study is deliberately focused on isolating the fundamental interactions between Ce^{4+} ions and HNO_3 concentration. This approach allows for a clearer understanding of the primary corrosion accelerant in the mainstream PUREX process, without the confounding variables introduced by multiple acid systems.

000Cr25Ni20 steel (C25) has demonstrated enhanced IGC resistance through the reduction of impurity elements (such as C, P, and Mn) and its high Cr and Ni content [14, 15]. However, research on the influence of Ce^{4+} ions on the corrosion resistance of C25 in SNFR environments remains limited, thereby constraining its practical application in environments containing Ce^{4+} ions. Therefore, C25 was selected as the research material in this study, and its corrosion behavior was systematically investigated in boiling nitric acid solutions with varying Ce^{4+} concentrations. 304L SS was chosen as the comparative material, as it is the most fundamental and widely utilized structural material in SNFR plants [4]. A detailed comparison of the corrosion characteristics between C25 and 304L SS was conducted to evaluate the performance of C25 in the same environment. Furthermore, the influence of HNO_3 concentrations (3, 6, and 10 mol/L) on the corrosion behavior of both materials in solutions with Ce^{4+} ions was explored, and the synergistic mechanism between HNO_3 concentration and Ce^{4+} ions was elucidated. This research will provide critical data to support the selection of structural materials for SNFR plants and establish the theoretical foundation for the development of a new generation of corrosion-resistant materials.

2 Material and methods

2.1 Materials and solution

The study employed C25 and 304L SS with solution-annealed treatment, whose chemical compositions are detailed in Table 1. Custom-designed "T" shaped samples were fabricated for electrochemical tests in boiling HNO_3 environments, as shown in Figure 1. The front segment of the "T" shaped sample serves as the testing area, with dimensions of 10 mm × 10 mm × 4 mm. The exposed area of each electrochemical sample was approximately 3.3 cm^2. The preparation of electrochemical samples adopted the laser spot welding technique to connect the copper wire with the tail of the "T" shaped sample. The electrode sealing process employed a hierarchical packaging approach: initially, primary packaging was achieved through high-temperature sintering with Teflon hoses, followed by secondary, localized encapsulation using Teflon sleeves. Samples with dimensions of 20 mm × 20 mm × 3 mm were prepared for corrosion weight loss measurements and characterization of corrosion morphology. All specimens were sequentially ground to #800 grit using silicon carbide paper, followed by ultrasonic cleaning in deionized water and ethanol, then dried with cold air from a blower before testing.

The nitric acid concentrations employed in this study were 3, 6, and 10 mol/L HNO_3, selected to represent the typical conditions commonly encountered in actual SNFR environments. These different concentrations of nitric acid

Table 1. Chemical compositions of C25 and 304L SS (wt.%).

Materials	C	Cr	Mn	Ni	P	S	Si	Fe
C25	≤0.005	24.80	0.34	21.54	≤0.005	≤0.005	<0.05	Balance
304L	0.037	18.16	1.21	8.16	0.029	0.003	0.41	Balance

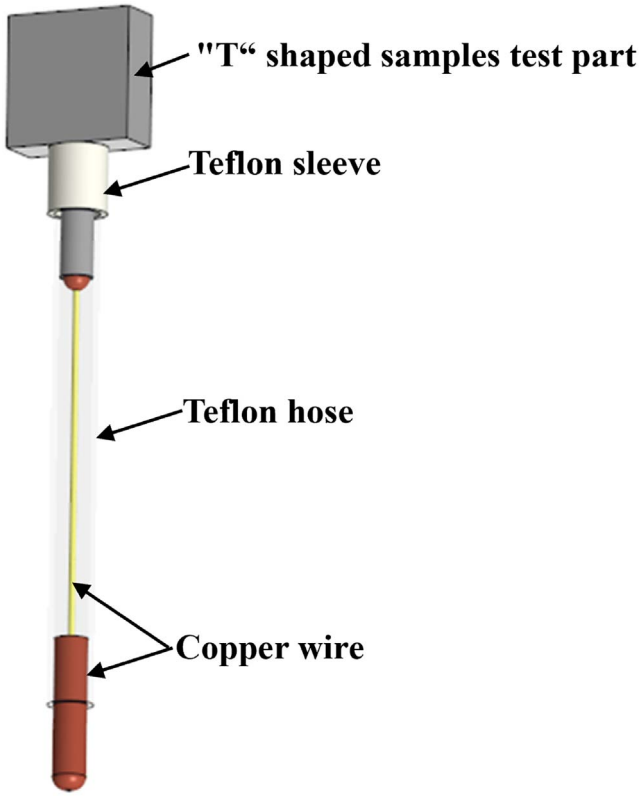

Fig. 1. Schematic diagrams of the electrochemical sample.

solutions were prepared by diluting 65 wt.% HNO_3 with deionized water. Analytical-grade $Ce(NH_4)_2(NO_3)_6$ was added as a Ce^{4+} source. The Ce^{4+} ion concentrations were chosen as 0.1 g/L, 1 g/L, and 5 g/L based on reprocessing plant data. All experiments were conducted at boiling temperature without prior deaeration. The boiling temperatures for 3, 6, and 10 mol/L HNO_3 were 104 ± 1 °C, 110 ± 1 °C, and 115 ± 1 °C, respectively.

2.2 Electrochemical tests

The electrochemical measurements were conducted in boiling 3, 6, and 10 mol/L HNO_3 solutions containing 0.1 g/L, 1 g/L, and 5 g/L Ce^{4+} ions, respectively. A three-electrode system was employed for electrochemical measurements. A schematic illustration of the experimental setup for electrochemical measurements in boiling nitric acid is provided in Figure 2. The sample acted as the working electrode (WE), a platinum foil as the counter electrode (CE), and a saturated calomel electrode (SCE) as the reference electrode (RE), connected to the electrolyte via a salt bridge with ceramic core holes at both ends. To ensure the accuracy of potential measurements, the SCE was calibrated before each experiment. After monitoring open circuit potential (OCP) for 30 minutes to ensure system stabilization, electrochemical impedance spectroscopy (EIS) was conducted from 0.1 Hz to 100 kHz by superimposing an AC voltage of 10 mV amplitude at OCP. Subsequently, potentiodynamic polarization (PD) was carried out from −300 mV vs. OCP to 1060 mV vs. SCE at a scan rate of 1 mV/s. All experiments were executed using a Reference 620 potentiostat (Gamry Instruments), and data were analyzed with Gamry Echem Analyst software.

2.3 Corrosion weight loss measurement

Corrosion weight loss measurements were performed according to the JB/T 7901-1999 standard. C25 and 304L SS samples were immersed in boiling 6 mol/L HNO_3 solutions containing varying Ce^{4+} concentrations (0.1 g/L, 1 g/L, and 5 g/L). Each sample underwent five consecutive cycles, each lasting 48 h, for a total exposure time of 240 h. At the end of each cycle, the corroded samples were retrieved, thoroughly washed, dried, weighed, and then re-immersed in the test solution for the next cycle. The corrosion rate (CR, mm/y) was determined by Eq. (1):

$$CR = \frac{87600\Delta w}{\rho A T}, \tag{1}$$

where Δw represents the weight loss (g), ρ denotes the density of the sample (g/cm^3), A signifies the sample area (cm^2), and T is the exposure time (h). To confirm result reproducibility, three parallel samples were employed.

2.4 Characterization of corrosion morphology and composition

Scanning Electron Microscope (SEM, Quattro S, FEI, USA) coupled with Energy Dispersive Spectrometer (EDS, Elect Super) was utilized to analyze the corrosion morphology and surface elemental compositions of C25 and 304L samples after immersion in boiling 6 mol/L HNO_3 solutions containing varying concentrations of Ce^{4+} ions (0.1 g/L, 1 g/L, and 5 g/L) for 240 h.

3 Results and discussion

3.1 Open circuit potential

The OCP results for C25 and 304L SS in boiling HNO_3 solution containing Ce^{4+} ions are presented in Figure 3. The results reveal that the OCP of both SS shifted to more positive values with increasing Ce^{4+} concentration in 3, 6, and 10 mol/L HNO_3 solutions. By contrast, variations in

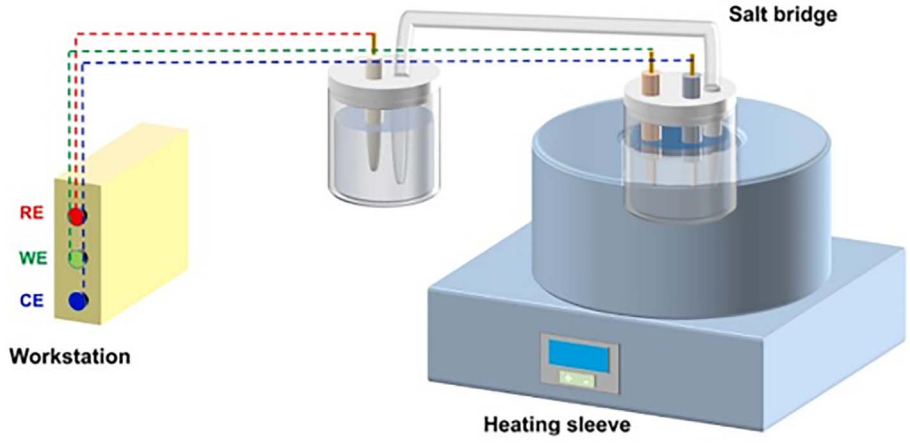

Fig. 2. Schematic diagram of boiling nitric acid electrochemical measurement device [16].

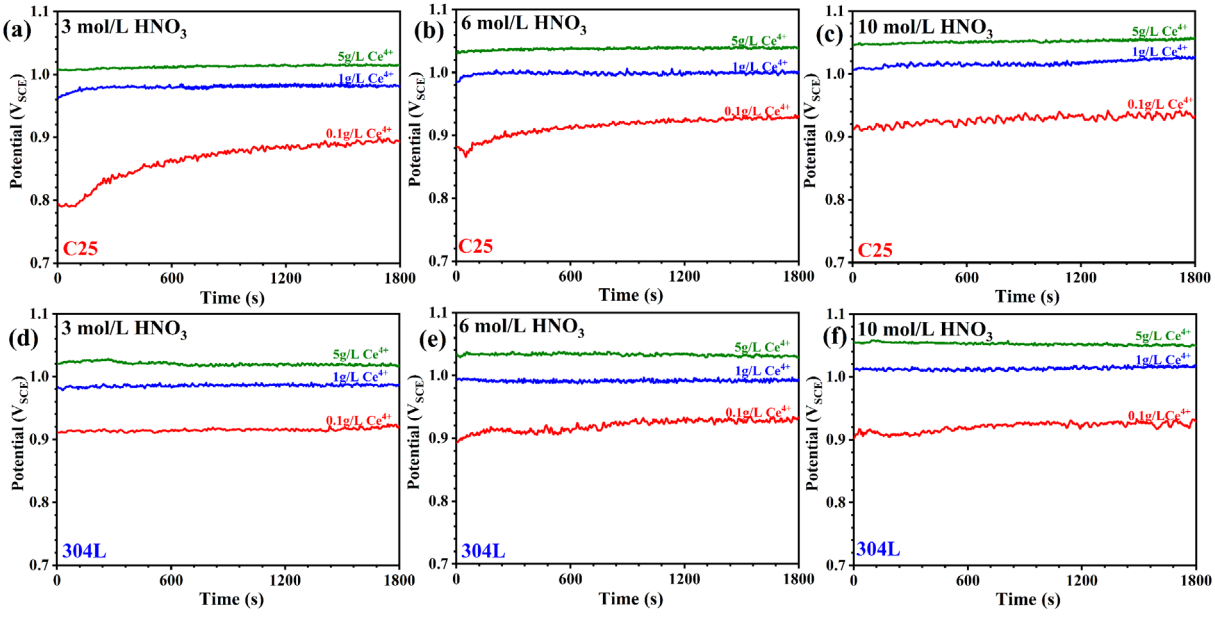

Fig. 3. OCP results of C25 and 304L SS in boiling (a, d) 3 mol/L, (b, e) 6 mol/L, and (c, f) 10 mol/L HNO_3 solutions containing Ce^{4+} ions.

HNO_3 concentration had a relatively limited impact on the OCP of both SS, which were significantly smaller in magnitude compared to the changes induced by the increase in Ce^{4+} concentration.

3.2 Electrochemical impedance spectroscopy

The EIS results for C25 and 304L SS in boiling HNO_3 solution containing Ce^{4+} ions are shown in Figure 4. The Nyquist plots reveal that as the Ce^{4+} concentration increases, the impedance arc radius decreases monotonically, indicating a reduction in corrosion resistance for both SS with increasing Ce^{4+} concentrations. In HNO_3 solution with 0.1 g/L Ce^{4+}, both SS exhibit capacitive loop characteristics; however, significant inductive loops appeared in the low-frequency region at Ce^{4+} concentrations of 1 g/L and 5 g/L. Based on the above analysis, the EIS data were further analyzed and fitted using the equivalent circuit (EC) models shown in Figures 5a–5b. The definition of each parameter in the EC is as follows: R_s represents the solution resistance; R_f and CPE_f represent the film resistance and film capacitance, respectively; R_{ct} and CPE_{dl} represent the charge-transfer resistance and double-layer capacitance, respectively; and L represents the inductive element. To account for the influence of electrode interfacial roughness on capacitive behavior, a constant phase element (CPE) was employed instead of a pure capacitive element [16, 17]. EC-1 was used to fit the EIS data in the HNO_3 solution containing 0.1 g/L Ce^{4+} ions, whereas EC-2 was used to fit the EIS data exhibiting low-frequency inductive

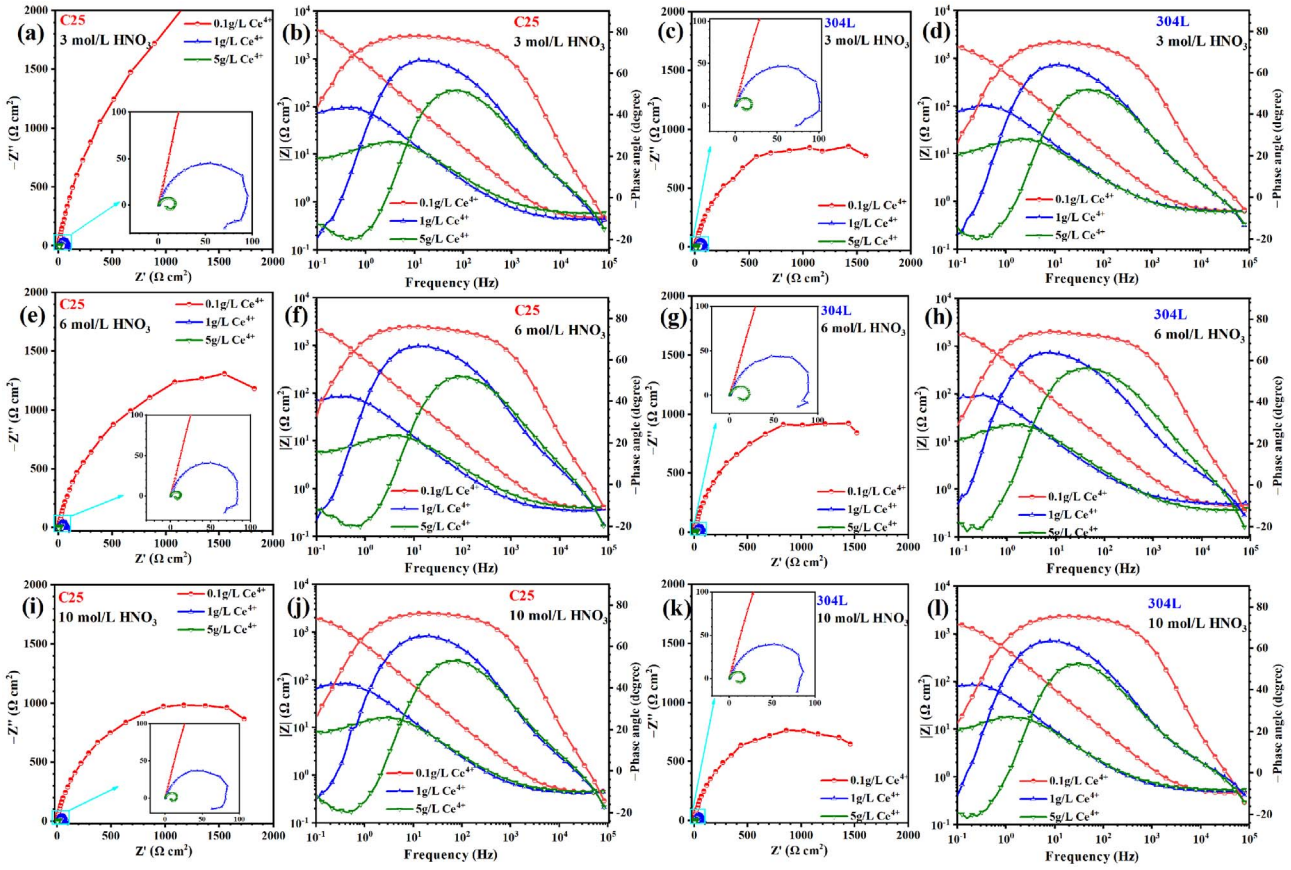

Fig. 4. EIS results of C25 and 304L SS in (a–d) 3 mol/L, (e–h) 6 mol/L, and (i–l) 10 mol/L boiling HNO_3 solutions containing Ce^{4+} ions.

behavior in HNO_3 solutions with Ce^{4+} concentrations of 1 g/L and 5 g/L. The appearance of inductive behavior at high Ce^{4+} concentrations (1 g/L and 5 g/L) is associated with adsorption/desorption processes or severe uniform/localized corrosion [18, 19], indicating a less protective surface film. The performance of the surface protection film can be evaluated by the polarization resistance (R_p), which is defined as $R_p = (Z_F)_{\omega=0}$, where Z_F and ω denote the faradaic impedance and angular frequency of the circuit, respectively. For EC-1 and EC-2, R_p can be expressed as $R_p = R_f + R_{ct}$ [20]. The calculated values of R_p for both SS in boiling HNO_3 solutions containing Ce^{4+} ions are presented in Figure 5c and Table 2. The results indicate that an increase in Ce^{4+} concentration leads to a monotonic decrease in R_p, while no clear regularity is observed in the effect of HNO_3 concentration on R_p values. Based on the EIS results, it can be conclusively inferred that the R_p values quantitatively demonstrate that Ce^{4+} ions accelerate the corrosion process of C25 and 304L SS in HNO_3 solution.

3.3 Potentiodynamic polarization

The PD curves of C25 and 304L SS in boiling HNO_3 solutions containing Ce^{4+} ions are presented in Figures 6a–6f. The corrosion potentials (E_{corr}) and current densities (I_{corr}) derived from PD curve fitting are illustrated in Figures 6g, 6h, and Table 2. In HNO_3 solutions with 0.1 g/L Ce^{4+}, I_{corr} was determined by cathodic Tafel fitting (−100 mV to −150 mV vs. E_{corr}); whereas, in HNO_3 solutions containing 1 g/L and 5 g/L Ce^{4+}, the cathodic curves of both SS exhibited pronounced diffusion-controlled characteristics. Therefore, the limiting diffusion current density was adopted as I_{corr} since the Tafel fitting was no longer applicable [21]. As depicted in Figure 6, the anodic process of both SS is largely unaffected by increasing Ce^{4+} concentration, whereas the cathodic process accelerates markedly. Furthermore, at identical Ce^{4+} concentrations, variations in HNO_3 concentration have minimal influence on the E_{corr} and I_{corr} of both SS, consistent with the I_{corr} trends reported by Ningshen [22] and Gopinath et al. [23] in pure HNO_3 solutions.

Next, we will explore the underlying reasons for this phenomenon. Before investigating the influence of Ce^{4+} on the cathodic behavior of stainless steel in HNO_3 solutions, it is crucial to attain a comprehensive understanding of the complex mechanism governing the cathodic reduction reaction during the corrosion of stainless steel in HNO_3 environments. Studies have demonstrated that in low-medium concentration HNO_3 (<8 mol/L), the autocatalytic reduction of HNO_3 ultimately produces NO [4, 24],

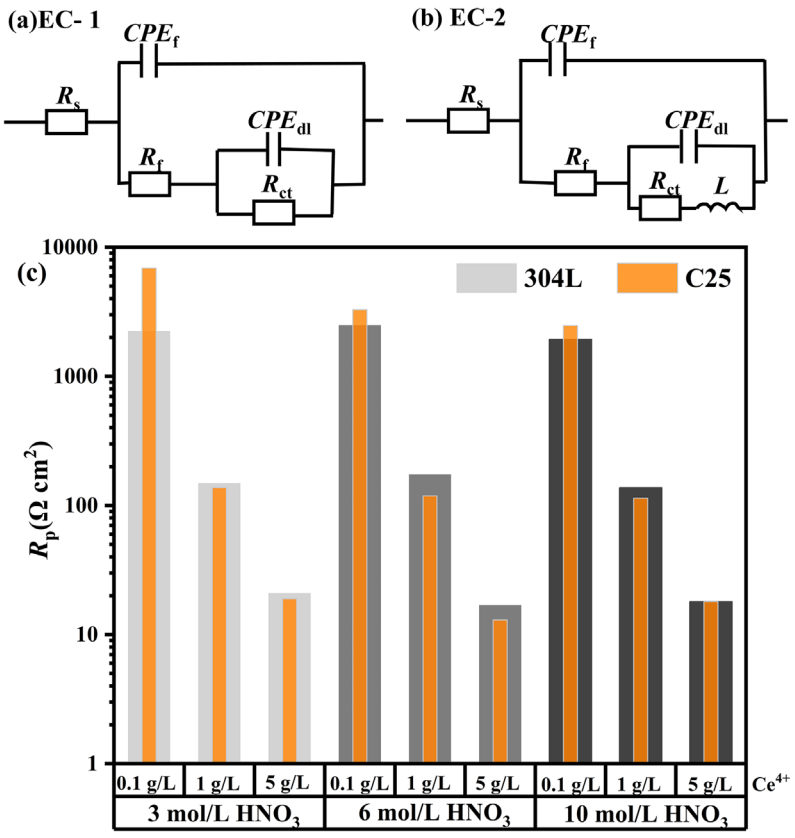

Fig. 5. (a, b) Equivalent circuit model for electrochemical impedance fitting. (c) R_p results of C25 and 304L SS obtained by fitting the EIS results.

Table 2. Summary of the corrosion parameters for C25 and 304L SS in boiling HNO_3 solutions with different Ce^{4+}

Materials	HNO_3 (mol/L)	Ce^{4+} (g/L)	R_p (Ω·cm^2)	E_{corr} (V vs. SCE)	I_{corr} (μA/cm^2)	Corrosion rate (240 h, mm/y)
C25	3	0.1	6901	905.4	2.843	–
C25	3	1	138	990.4	355	–
C25	3	5	19	1019	2512	–
C25	6	0.1	3283	949.3	7.418	0.021
C25	6	1	119	1009	393.2	0.155
C25	6	5	13	1040	3595	0.826
C25	10	0.1	2474	932.1	7.535	–
C25	10	1	114	1032	455	–
C25	10	5	18	1060	3359	–
304L	3	0.1	2246	934.2	12.47	–
304L	3	1	149	992.9	364.3	–
304L	3	5	21	1018	2537	–
304L	6	0.1	2498	934.5	13.85	0.051
304L	6	1	175	999.5	460.2	0.24
304L	6	5	17	1036	3982	1.206
304L	10	0.1	1930	923.2	13.72	–
304L	10	1	137	1024	478.8	–
304L	10	5	18	1048	3628	–

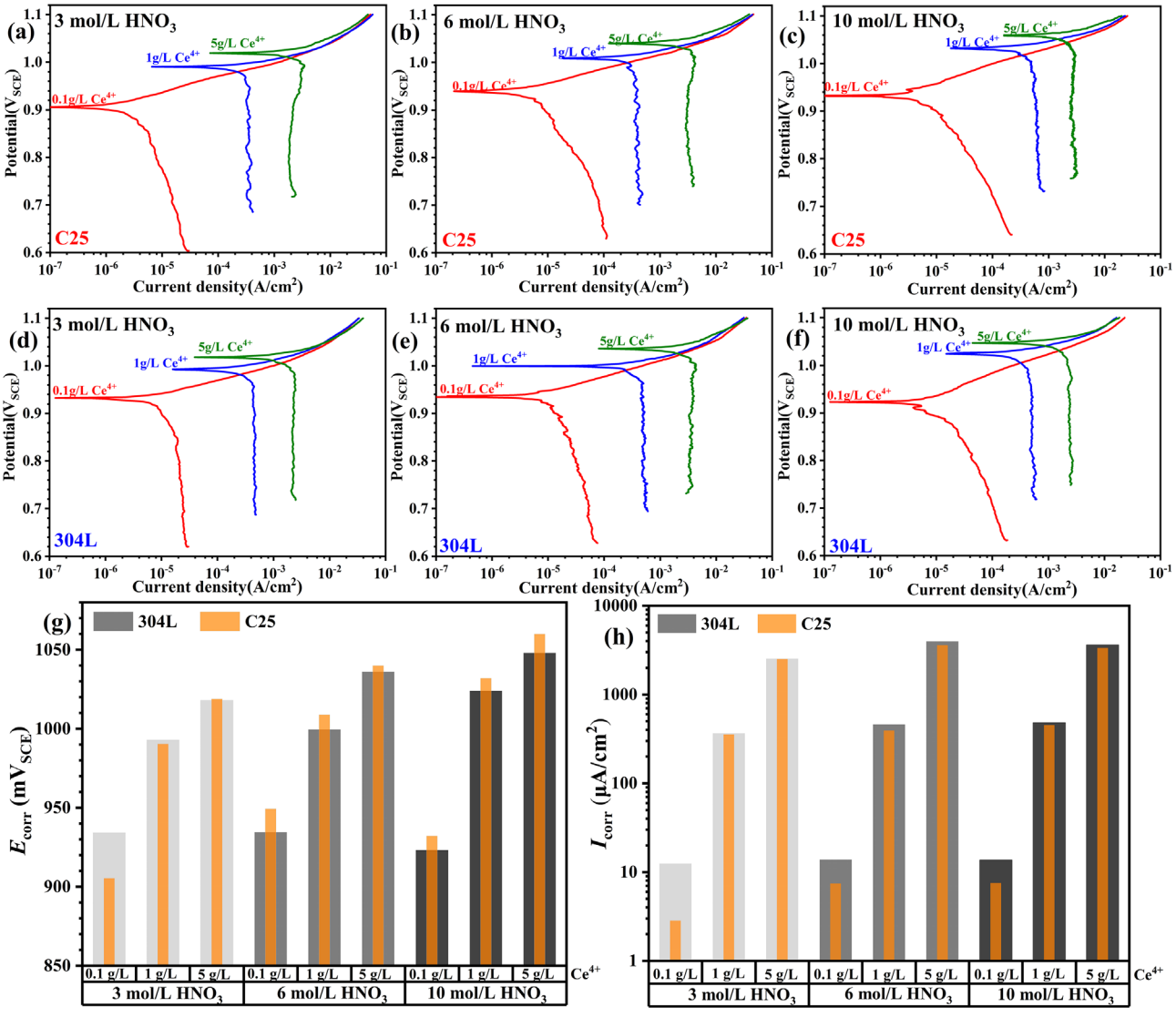

Fig 6. PD curves of C25 and 304L SS in (a, d) 3 mol/L, (b, e) 6 mol/L, and (c, f) 10 mol/L boiling HNO_3 solutions containing Ce^{4+} ions. (g) E_{corr} and (h) I_{corr} values obtained by cathodic fitting of the PD curves.

with its reduction process following Eqs. (2)–(4). Specifically, the redox potential of the HNO_3 solution is predominantly determined by the reduction reaction of HNO_3:

$$NO_3^- + 3H^+2e^- \rightarrow HNO_2 + H_2O \quad \left(\Delta E^{\Theta}_{25\,^{\circ}C} = 934\,\text{mV/SHE}\right) \tag{2}$$

Subsequently, the electrochemically active species HNO_2 is further reduced to form NO:

$$(HNO_2)_{el} + H^+ + e^- + s \rightarrow (NO)_{ads} + H_2O \quad (\text{s denotes the active site at the electrode}) \tag{3}$$

In addition, regeneration of HNO_2 is achieved by a chemical reaction between HNO_3 and NO:

$$HNO_3 + 2(NO)_{ads} + H_2O \rightarrow 3(HNO_2)_{ads} + 2s \tag{4}$$

Conversely, in highly concentrated HNO_3 (>8 mol/L), the cathodic reduction of HNO_3 is primarily governed by Eqs. (2) and (3) and (5) and (6), with NO_2 emerging as the ultimate reduction product:

$$HNO_3 + (NO)_{ads} \rightarrow (HNO_2)_{el} + (NO_2)_{ads} \tag{5}$$

$$HNO_3 + (HNO_2)_{el} + 2s \rightarrow 2(NO_2)_{ads} + H_2O \tag{6}$$

The HNO_3 reduction process can be rapidly facilitated through an autocatalytic mechanism that involves both electrochemical and chemical reactions. However, the reduction of Ce^{4+} ions in HNO_3 solution follows Eq. (7) [25]:

$$Ce^{4+} + e^- \rightarrow Ce^{3+} \quad \left(\Delta E^{\Theta}_{25\,^{\circ}C} = 1610\,\text{mV/SHE}\right) \tag{7}$$

It is worth noting that the redox potential of Ce^{4+} ions in HNO_3 solution (1610 mV/SHE) is significantly higher than

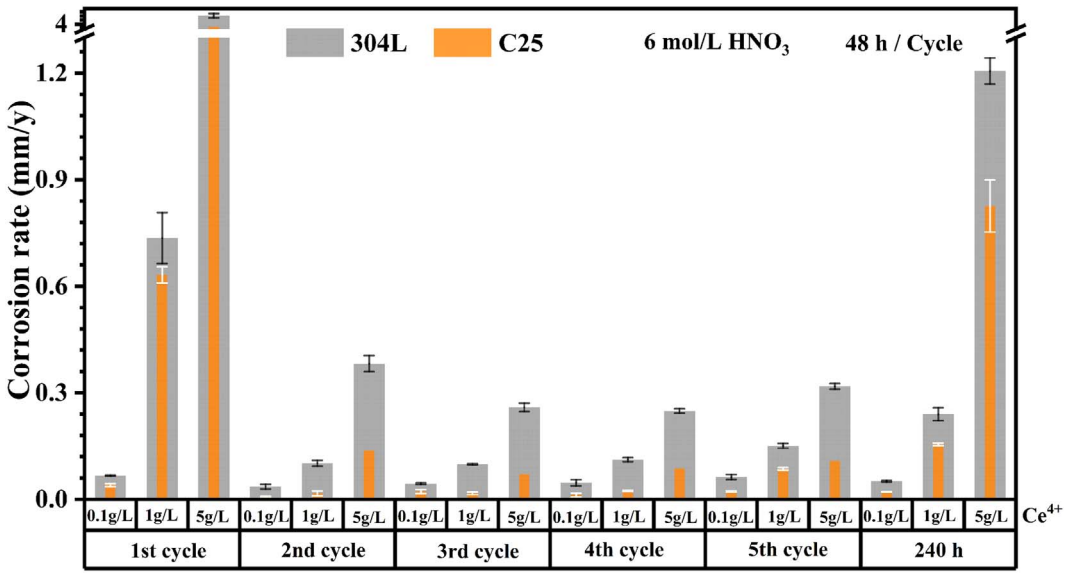

Fig 7. Corrosion rate of C25 and 304L SS in 6 mol/L boiling HNO_3 solutions containing Ce^{4+} ions for each cycle (48 h/cycle) and 240 h.

that of HNO_3 (934 mV/SHE). Based on the mixed potential theory [26], the higher redox potential allows Ce^{4+} ions to be preferentially reduced during the cathodic process compared to HNO_3, thereby accelerating the cathodic reaction rate for both SS after the addition of Ce^{4+} ions. As depicted in Figures 6a–6f, the anodic process of both SS remains largely unchanged, while the cathodic process is markedly accelerated with increasing Ce^{4+} concentration. Consequently, E_{corr} shifts toward the transpassive region (Fig. 6g), leading to a substantial increase in I_{corr} (Fig. 6h). Under transpassive conditions, the insoluble Cr_2O_3 passive film of stainless steel becomes unstable and dissolves preferentially in the form of soluble chromate species, such as CrO_4^{2-} or $Cr_2O_7^{2-}$ [4, 12, 27]. This transpassive dissolution is particularly pronounced at grain boundaries characterized by higher energy states [4]. The localized breakdown of the passive film at these sites initiates corrosion attack, which rapidly propagates along grain boundaries, resulting in IGC [5, 19]. Therefore, Ce^{4+}-induced cathodic acceleration, together with the consequent positive shift in E_{corr}, enhances IGC susceptibility by promoting selective transpassive dissolution at grain boundaries.

Although increasing HNO_3 concentration can promote its autocatalytic reduction, in the presence of Ce^{4+}, the primary cathodic reaction for both SS involves the reduction of Ce^{4+} ions (Eq. (7)). Consequently, in an environment containing strongly oxidizing Ce^{4+} ions, increasing the HNO_3 concentration does not significantly influence the cathodic process or greatly accelerate the corrosion of both SS. This elucidates why increasing the HNO_3 concentration has minimal impact on E_{corr}, I_{corr}, and R_p for both SS in a solution with Ce^{4+} ions, indicating limited effects on the short-term corrosion behavior of C25 and 304L SS.

3.4 Corrosion weight loss measurement

Subsequently, long-term corrosion weight loss experiments were conducted to further evaluate the effect of Ce^{4+} ions on the corrosion resistance of C25 and 304L SS in HNO_3 solution. Given that electrochemical results demonstrated minimal effect of HNO_3 concentration on corrosion behavior in the presence of Ce^{4+}, weight loss tests were performed exclusively in 6 mol/L HNO_3 with varying concentrations of Ce^{4+}, without extending to different acid concentrations. The focus on 6 mol/L HNO_3 was justified by its relevance as a representative condition in continuous dissolvers used for stainless steel in nuclear reprocessing plants [3, 22]. In contrast, electrochemical tests encompassed a broader range of HNO_3 concentrations to elucidate general corrosion trends. As demonstrated in Figure 7, both SS underwent five cycles (each lasting 48 h) of corrosion testing in boiling 6 mol/L HNO_3 solutions containing Ce^{4+} ions over a total duration of 240 h. The results revealed that the corrosion rates of both SS increased monotonically with increasing Ce^{4+} concentration, confirming that Ce^{4+} ions significantly accelerate the corrosion process of both SS. In practical operations within SNFR plants, continuous monitoring of Ce^{4+} concentration is critical to prevent IGC induced by Ce^{4+} ions. Furthermore, the corrosion rates of C25 and 304L SS exhibited the highest corrosion rate during the first cycle, followed by stabilization over the subsequent four cycles, suggesting that the initial 48-hour period corresponds to the rapid initiation phase of corrosion. Notably, under identical solution conditions, the corrosion rate of C25 was consistently lower than that of 304L SS, demonstrating the superior corrosion resistance of C25, which can be attributed to its higher Cr and Ni contents and reduced impurity levels.

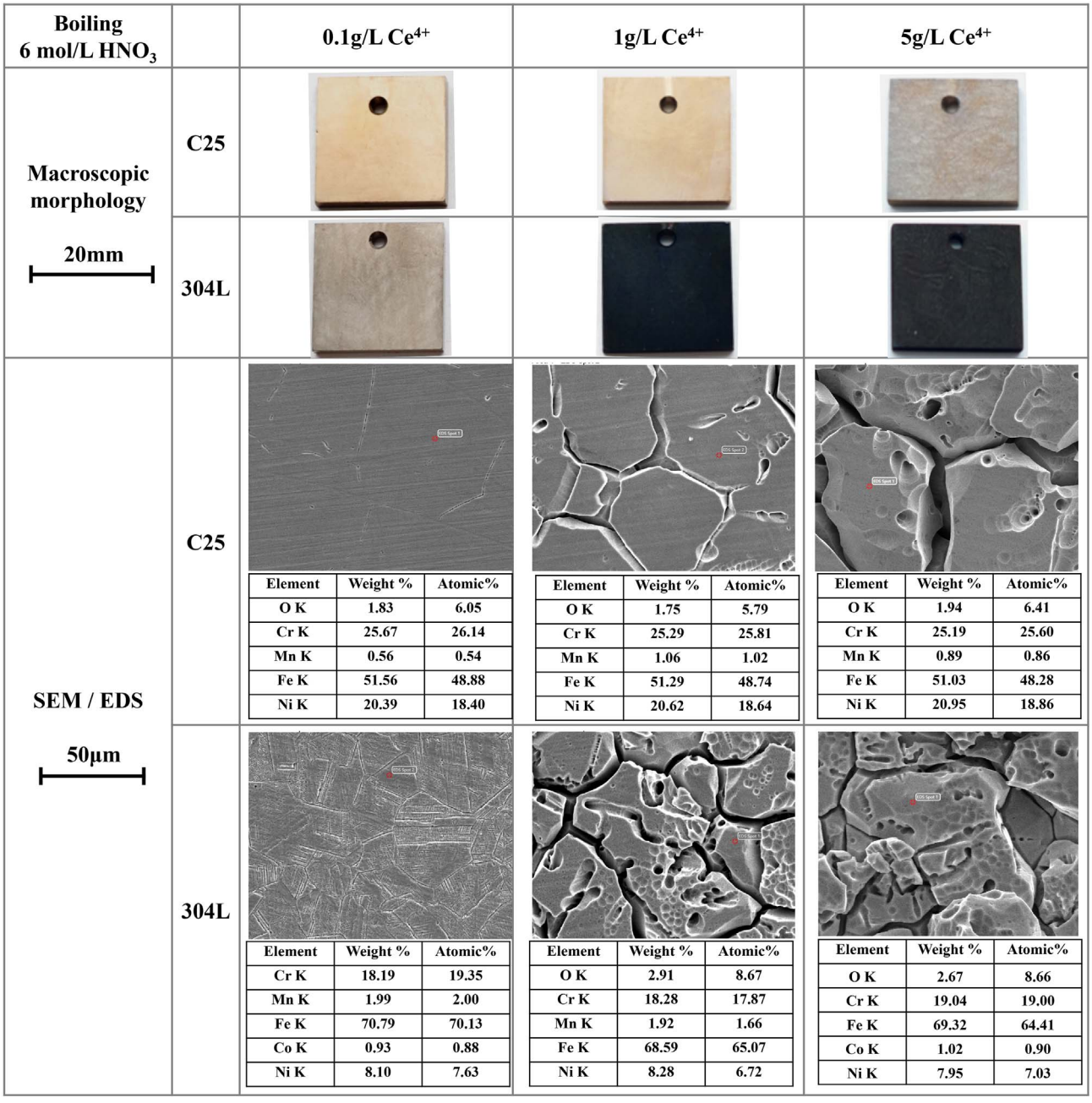

Fig. 8. Morphology and elemental compositions of the corrosion films formed on C25 and 304L SS after 240 h of immersion in a boiling 6 mol/L HNO_3 solution containing Ce^{4+} ions.

3.5 Corrosion morphology and elemental composition

After C25 and 304L SS were immersed in boiling 6 mol/L HNO_3 solution containing Ce^{4+} ions for 240 h, the surface corrosion morphology and EDS elemental composition results are presented in Figure 8. In the HNO_3 solution with a Ce^{4+} concentration of 0.1 g/L, C25 did not exhibit typical IGC, whereas 304L SS showed slight IGC along with intragranular corrosion. When the Ce^{4+} concentration was increased to 1 g/L, IGC began to appear on the C25 surface, and the degree of IGC on 304L SS became more pronounced. Upon further increasing the Ce^{4+} concentration to 5 g/L, the IGC of both SS was significantly exacerbated, as indicated by deeper and wider grooves in the grain boundary regions. However, EDS analysis revealed that Ce^{4+} ions had no significant effect on the elemental composition of the corroded surfaces.

4 Conclusion

This study systematically investigated the corrosion behavior of C25 and 304L SS in boiling HNO_3 solutions containing Ce^{4+} ions through electrochemical tests, weight loss

measurements, and surface characterization. The effects of Ce^{4+} concentration and HNO_3 concentration on the corrosion behavior of both SS were systematically evaluated. The core findings are as follows:

1. Ce^{4+} ions significantly degrade the corrosion resistance of both SS. With increasing Ce^{4+} concentration, E_{corr} shifts positively, I_{corr} increases, and R_p decreases. Weight loss tests further confirm that higher Ce^{4+} concentrations lead to monotonically increased corrosion rates and exacerbated IGC, attributed to Ce^{4+}-accelerated cathodic reduction driving E_{corr} into the transpassive region. Nevertheless, Ce^{4+} ions in solution do not alter the composition of the corroded surface film.
2. In the presence of Ce^{4+} ions, variations in HNO_3 concentration (3, 6, and 10 mol/L) exert a relatively minor influence on the E_{corr}, I_{corr}, and R_p values for C25 and 304L SS. This indicates that Ce^{4+} (as a strong oxidizing cation) dominates over HNO_3 concentration in regulating short-term corrosion behavior.
3. Both C25 and 304L SS exhibit the highest corrosion rates in the initial 48-hour cycle, followed by a decrease and stabilization in the subsequent four cycles. C25 demonstrates superior corrosion resistance compared to 304L SS due to its higher Cr and Ni contents and lower impurity levels, making it a promising candidate for fabricating SNFR equipment requiring higher corrosion resistance than 304L SS.

Funding

This research was funded by National Natural Science Foundation of China (52373321), IMR Innovation Fund (2023-PY03) and LingChuang Research Project of China National Nuclear Corporation (CNNC-LCKY-202274).

Conflicts of interest

The authors have nothing to disclose.

Data availability statement

Data will be made available on request.

Author contribution statement

Conceptualization, Aili Ma; Methodology, Aili Ma; Investigation, Qiqian Chen; Formal Analysis, Qiqian Chen, and Lianmin Zhang; Writing – Original Draft Preparation, Qiqian Chen; Writing – Review & Editing, Aili Ma and Lianmin Zhang; Supervision, Yugui Zheng.

References

1 Z. Liu, L.M. Zhang, C.C. Liu, K.D. Tan, A.L. Ma, Y.G. Zheng, Understanding of tribocorrosion and corrosion characteristics of 304L stainless steel in hot concentrated nitric acid solution, *J. Cent. South Univ.* **31,** 3657–3673 (2024). https://doi.org/10.1007/s11771-024-5764-7.

2 R.D. Shaw, Corrosion prevention and control at Sellafield nuclear fuel reprocessing plant, *Br. Corros. J* **25**, 97–107 (1990). https://doi.org/10.1179/000705990798269676.

3 F. Balbaud-Célérier, N. Gruet, B. Gwinner, P. Laghoutaris, Corrosion behavior of stainless steels in nitric acid in the context of nuclear fuel reprocessing plants, *Nuclear Corrosion* **69**, 301–340 (2020). https://doi.org/10.1016/b978-0-12-823719-9.00008-1.

4 P. Fauvet, F. Balbaud, R. Robin, Q.T. Tran, A. Mugnier, D. Espinoux, Corrosion mechanisms of austenitic stainless steels in nitric media used in reprocessing plants, *J. Nucl. Mater.* **375**, 52–64 (2008). https://doi.org/10.1016/j.jnucmat.2007.10.017.

5 E. Irisawa, M. Yamamoto, C. Kato, T. Motooka, Y. Ban, Effect of re-oxidation rate of additive cations on corrosion rate of stainless steel in boiling nitric acid solution, *J. Nucl. Sci. Technol.* **56**, 337–344 (2019). https://doi.org/10.1080/00223131.2019.1580624.

6 S. Bhise, V. Kain, Methodology based on potential measurement for predicting corrosion behaviour of SS 304L in boiling nitric acid containing oxidising ions, *Corros. Eng. Sci. Technol.* **47**, 61–69 (2013). https://doi.org/10.1179/1743278211y.0000000016.

7 Z. Liu, L.M. Zhang, W.Q. Chen, A.L. Ma, Y. Zheng, W. Yan, Y.F. Li, E.F. Daniel, Y.Y. Shan, Y.G. Zheng, Effect of oxidizing ions on the corrosion behavior of SiN stainless steel in high-temperature nitric acid solution, *Electrochim. Acta* **442**, 141917 (2023). https://doi.org/10.1016/j.electacta.2023.141917.

8 T. Yamamoto, S. Tsukui, S. Okamoto, T. Nagai, M. Takeuchi, S. Takeda, Y. Tanaka, Gamma-ray irradiation effects on corrosion rates of stainless steel in boiling nitric acid containing ionic additives, *J. Nucl. Sci. Technol.* **35**, 353–356 (2012). https://doi.org/10.1080/18811248.1998.9733871.

9 R. Priya, S. Ningshen, The tribocorrosion behaviour and its mechanisms of type 304L stainless steel in nitric acid media, *J. Mater. Eng. Perform.* **32**, 5261–5272 (2023). https://doi.org/10.1007/s11665-022-07511-y.

10 H. Badet, F. Poineau, Corrosion studies of stainless steel 304 L in nitric acid in the presence of uranyl nitrate: effect of temperature and nitric acid concentration, *SN Appl. Sci.* **2**, 459 (2020). https://doi.org/10.1007/s42452-020-2273-7.

11 G. Shit, S. Ningshen, Effect of metallic redox ions on the corrosion behavior of GTAW weldment of type 304L stainless steel in simulated non-radioactive PUREX and HLLW medium, *Prog. Nucl. Energy* **168**, 105039 (2024). https://doi.org/10.1016/j.pnucene.2023.105039.

12 B. Raj, U.K. Mudali, Materials development and corrosion problems in nuclear fuel reprocessing plants, *Prog. Nucl. Energy* **48**, 283–313 (2006). https://doi.org/10.1016/j.pnucene.2005.07.001.

13 C. Padovani, The corrosion behavior of stainless steel in conditions relevant to the storage of intermediate level radioactive waste, in *Nuclear Corrosion*, edited by S. Ritter (Woodhead Publishing, 2020), pp. 341–370.

14 W. Wang, M. Luo, Q.F. Zhang, J.Q. Zhao, Corrosion resistance of 000Cr25Ni20 stainless steel in boiling and non-boiling nitric acid containing Cr6+, Run+. *Material Protection* (in Chinese) **42**, 19–21 (2009). https://doi.org/10.16577/j.cnki.42-1215/tb.2009.02.009.

15 W. Wang, M. Luo, Q.F. Zhang, Effect of silicon on the corrosion resistance of austenitic stainless steels in boiling nitric acid containing strong oxidising ions, *J. Iron Steel Res.*

(in Chinese) **21**, 41–45 (2009). https://doi.org/10.13228/j.boyuan.issn1001-0963.2009.08.003.
16 Z. Liu, L.M. Zhang, W.Q. Chen, A.L. Ma, Y. Zheng, W. Yan, Y.F. Li, Y.Y. Shan, X.W. Hu, C. Kan, Y.G. Zheng, Effect of chloride ion on the corrosion behavior of SiN stainless steel in concentrated hot nitric acid media, *Corros. Sci.* **225**, (2023). https://doi.org/10.1016/j.corsci.2023.111604.
17 C.C. Liu, L.M. Zhang, Z. Liu, A.L. Ma, Z.X. Liu, Y.G. Zheng, Exploring the impact of Al alloying on microstructure and hot nitric acid corrosion resistance of Ti-xAl (x=0, 1, 2, 3, 4, 5) alloys, *Corros. Sci.* **232**, (2024). https://doi.org/10.1016/j.corsci.2024.112010.
18 S.E. Lemallem, A. Fiala, H.B. Ladouani, H. Allal, Corrosion inhibition performance of two ketene dithioacetal derivatives for stainless steel in hydrochloric acid solution, *J. Electrochem. Sci. Technol.* **13**, 237–253 (2022). https://doi.org/10.33961/jecst.2021.00822.
19 K. Morshed Behbahani, P. Najafisayar, M. Pakshir, Study of the intergranular corrosion of sensitized UNS S31803 stainless steel in transpassive region, *J. Mater. Eng. Perform* **25**, 3418–3429 (2016). https://doi.org/10.1007/s11665-016-2176-3.
20 Z.Q. Zheng, J.C. Lu, Z.B. Wang, Y. Zhao, B. He, Y.G. Zheng, Improving corrosion resistance of copper-nickel alloys by the microalloying-facilitated formation of protective corrosion product films, *Corros. Sci.* **245**, (2025). https://doi.org/10.1016/j.corsci.2025.112693.
21 L. Pang, Z.B. Wang, M.H. Lu, Y. Lu, X. Liu, Y.G. Zheng, Inhibition performance of benzimidazole derivatives with different heteroatoms on the under-deposit corrosion of carbon steel in CO_2-saturated solution, *Corros. Sci.* **192**, (2021). https://doi.org/10.1016/j.corsci.2021.109841.
22 S. Ningshen, M. Sakairi, Corrosion degradation of AISI type 304L stainless steel for application in nuclear reprocessing plant, *J. Solid State Electrochem.* **19**, 3533–3542 (2015). https://doi.org/10.1007/s10008-015-2891-y.
23 G. Shit, S. Ningshen, The corrosion behavior of compositional modified AISI type 304L stainless steel for nitric acid application, *Anti-Corros. Methods Mater.* **66**, 149–158 (2019). https://doi.org/10.1108/acmm-02-2018-1906.
24 D. Sicsic, F. Balbaud-Célérier, B. Tribollet, Mechanism of nitric acid reduction and kinetic modelling, *Eur. J. Inorg. Chem.* **2014**, 6174–6184 (2014). https://doi.org/10.1002/ejic.201402708.
25 P.K. Sinha, V. Kain, Superior corrosion resistance of Ti-Al-Zr alloy in aggressive nitric acid environments, *J. Mater. Eng. Perform.* **29**, 8441–8450 (2020). https://doi.org/10.1007/s11665-020-05300-z.
26 Y. Zheng, S. Luo, W. Ke, Effect of passivity on electrochemical corrosion behavior of alloys during cavitation in aqueous solutions, *Wear* **262**, 1308–1314 (2007). https://doi.org/10.1016/j.wear.2007.01.006.
27 G. Shit, A. Poonguzhali, S. Ningshen, Improvement of intergranular corrosion resistance of SS 304L by grain refinement followed by gamma-ray irradiation treatment for the application in the back end of the nuclear fuel cycle, *Mater. Chem. Phys.* **313**, 128750 (2024). https://doi.org/10.1016/j.matchemphys.2023.128750.

Cite this article as: Chen Q, Ma A, Zhang L & Zheng Y. Corrosion behavior of 000Cr25Ni20 and 304L stainless steels in boiling nitric acid solutions containing Ce^{4+} ions, Res. Des. Nucl. Eng. **1**, 2025009 (2025), https://doi.org/10.1051/rdne/2025009.